Check for
updates

Structural, vibrational, quantum chemical calculations, thermal and antimicrobial studies on nitrate salt of 3-nitroaniline

S. Thangarasu[1,2] · V. Siva[1,2] · S. Asath Bahadur[1,2] · S. Athimoolam[3]

© The Author(s), under exclusive licence to Springer Science+Business Media, LLC, part of Springer Nature 2021

Abstract
In this work, 3-nitroanilinium nitrate (3NAN) has been synthesized and crystallized successfully by solution growth combined with solvent evaporation technique. 3NAN molecular structure has been optimized with Density Functional Theory (DFT) using B3LYP function and Hartree–Fock method with a $6–311++G(d,p)$ basis set. The geometrical parameters of the title molecules have been analyzed. The computed vibrational spectra were compared with experimental result which show appreciable agreement. Thermal stability of the crystal was analyzed with TGA/DTA and the melting points of the salt identified at 209 ºC. HOMO–LUMO energy calculations have shown the charge transfer within the molecule. The possible pharmaceutical/biological activity of the salts confirmed by the Frontier Molecular Orbital (FMO) analysis have lower band gap value. The antimicrobial activity of grown crystals has been tested against certain potentially threatening microbes.

Keywords DFT · Vibrational assignments · HOMO–LUMO · TG–DTA · Antimicrobial activity

1 Introduction

Generally nitroaniline is called as push–pull molecule. Because of the intramolecular charge transfer (ICT) from the –NH$_2$ (electron-donor group) to –NO$_2$ (electron-acceptor group) through the phenyl ring. 3-Nitroaniline and 4-nitroaniline are used as reference compounds for optical nonlinearity (Krishnakumar et al. 2008; Bishop et al. 1998; Reis et al. 2000) calculated by computational and experimental method. 3-Nitroaniline and its derivatives are biologically important compounds, such compounds are produced

✉ S. Thangarasu
  sthangarasu@gmail.com

1   Department of Physics, School of Advanced Sciences, Kalasalingam Academy of Research and Education, Krishnankoil 626 126, India

2   Condensed Matter Physics Laboratory, International Research Centre, Kalasalingam Academy of Research and Education, Krishnankoil 626 126, India

3   Department of Physics, Anna University, University College of Engineering, Nagercoil 629 004, India

significant antihyperglycemic as well as hypoglycemic effects in alloxan-induced and nor-mal diabetic rabbits (Jain et al. 2005). Also m-Nitroaniline plays an essential role in sev-eral biological processes and has considerable chemical and pharmacological importance. Since a long time, schiff based compounds are generally considered due to their impor-tance in several electro-optical and other biological applications (Siva et al. 2019).

In this context, a new family of organic–inorganic crystals with the biological impor-tance, with chemical, physical and thermal properties through inorganic sub networks is proposed. Based on the above specifics, 3-nitroaniline was reacted with nitric acid and the crystals of 3-nitroanilinium nitrate were grown. In this paper, the synthesis, crystal growth, structural, spectroscopic, thermal analyses and biological activity of 3NAN is reported.

2 Experimental

2.1 Material preparation

3-nitroanilinium nitrate is synthesized from the AR grade 3-nitroaniline and nitric acid obtained from Himedia fine chemicals taken in 1:1 ratio using acetone, as solvent. This solution was stirred well for about 1 h to get clear solution filtered and kept in a clean beaker for evaporation. The title crystal was synthesized according to the scheme as shown in Fig. 1. The reaction was allowed in room temperature. After many attempts, the com-pound 3-nitroaniline nitrate has not yielded good quality single crystal; which is not suit-able for single crystal X-ray diffraction. Hence, the powder XRD analysis of 3NAN was taken to prove the new phase of the complex.

2.2 Characterization techniques

Powder XRD study of 3NAN was carried out by Bruker X-ray diffractometer of D8 advanced ECO XRD system with SSD160 1D Detector. The diffraction was collected in the range of 2θ, 0° to 50°. The preliminary data of the polycrystalline sample were calcu-lated by indexing in the first 2θ strong intensity peaks using DASH 3.3.2 program (David et al. 2006). FT-IR spectrum of grown crystal was recorded using Nexus 670 FTIR spec-trometer and FT-Raman spectrum were recorded using BRUKER RFS 27 FT-Raman Spec-trometer. Both the spectra were recorded in the range of 400 to 4000 cm^{-1} with Nd:YAG laser at 1064 nm as source. DTA/TGA of grown crystals were carried out by SII (SEIKO)
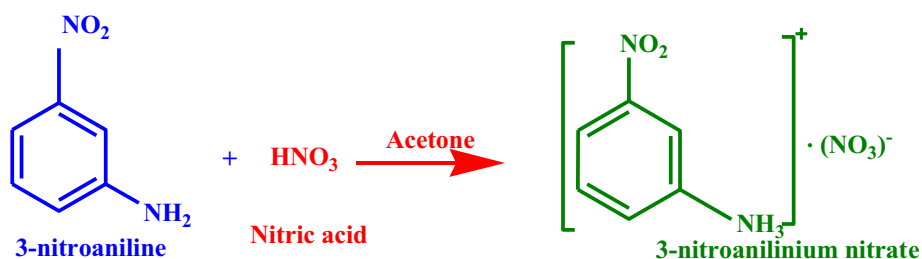

Fig. 1 Reaction scheme of 3-Nitroanilinium nitrate

Japan Analytical Instrument, Model No: TG/DTA-6200 in N_2 atmosphere with heating rate 20 °C/min.

2.3 Computational profile

The 3NAN molecular parameters in the ground state were computed by performing both HF and B3LYP with basis set 6–311 + G(d,p). Computational calculations were performed using GAUSSIAN 09 W (Frisch et al. 2010) program package on i5 processor/3.20 GHz personal computer without any constraint on the geometry (Schlegel 1982). The geometry of the title compound was optimized by the computational method. The HF and B3LYP method (Hohenberg and Kohn 1964) acknowledged as a practical approach for the computation of molecular structure and vibrational frequencies with the Becke's three parameter exact exchange-functional (B3)(Becke 1993) combined with gradient-corrected correlational functional of Lee, Yang and Parr (LYP) (Lee et al. 1988). Using principle of statistical mechanics, thermodynamic properties of 3NAN have been calculated from normal mode of vibrational frequencies which provide the details about title compound in gas phase. GAUSSVIEW program (Dennington et al. 2013) with symmetry considerations were used to assign vibrational frequencies. The HOMO–LUMO energies were calculated and computed by the HF and B3LYP method.

3 Results and discussion

3.1 Structural and molecular geometry analyses

The possible unit cell parameters for 3NAN is given in Table 1. By comparing the powder XRD pattern of grown crystal 3NAN compared with its pure 3-nitroaniline and shown in Fig. 2. With the help of XRD pattern and the unit cell values are confirmed the 3NAN salt formation. Some of the new intensity peaks are appear in 3NAN crystals and some of the peaks are disappear compared to 3-nitroaniline. The possible unit cell parameters were identified and 3NAN crystal belongs to orthorhombic system was notable using DASH 3.3.2 program.

In 3NAN, asymmetric part of unit cell contains 3-nitroaniline (cation) charge is neutralized with nitrate (anion). The optimized molecular structure of 3-nitroanilinium nitrate diagram and atom numbering scheme are shown in the Fig. 3 and geometrical parameters are given in Table 2. In phenyl ring, optimized C–C bond length

Table 1 Unit cell parameters of 3NAN

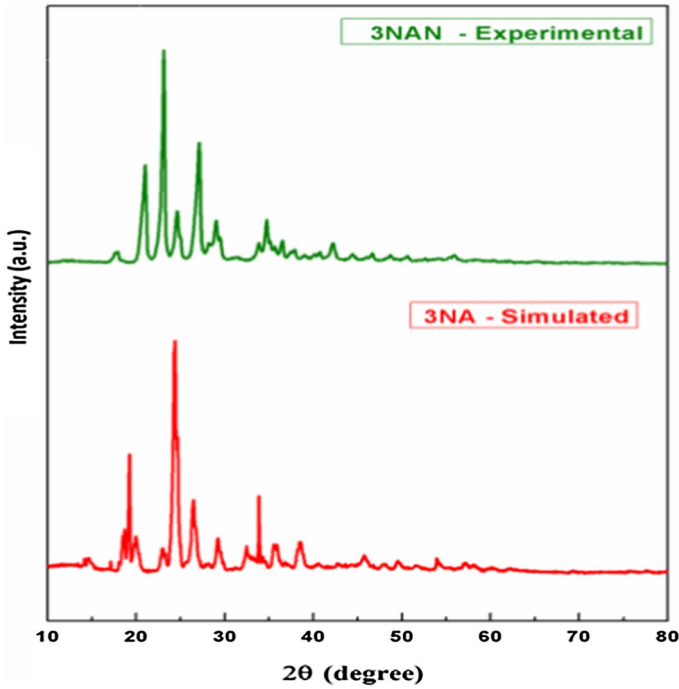| Unit cell Parameters	Values
a (Å)	21.486 (8)
b (Å)	19.163 (1)
c (Å)	3.884 (1)
α (°)	90
β (°)	90
γ (°)	90
Volume (Å^3)	1599.4

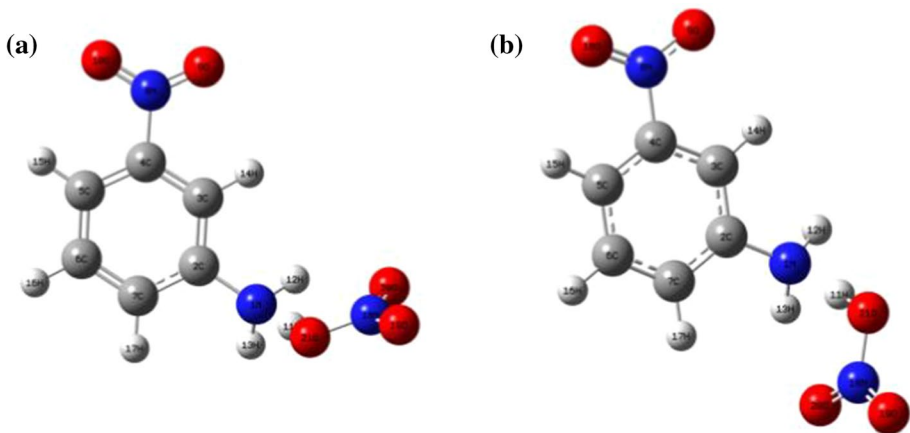**Fig. 2** Powder XRD patterns of 3NAN and 3NA

Fig. 3 Optimized molecular structure of 3NAN by **a** HF and **b** B3LYP method

is calculated by HF method around 1.381–1.390 Å and by B3LYP method around 1.389–1.400 Å. The N–O bond lengths are calculated around 1.167–1.321 Å by HF method and 1.199–1.382 Å by B3LYP method in nitrate anion.

Table 2 Optimized molecular geometrical parameters of 3NAN

Bond length (Å)	HF/6–311 + +(d,p)	B3LYP/6–311 + +(d,p)	Bond angle (°)	HF/6–311 + +(d,p)	B3LYP/6–311 + +(d,p)
N1–C2	1.414	1.422	N1–C2–C3	120.2	120.3
C4–N8	1.470	1.483	N1–C2–C7	120.3	120.1
C2–C3	1.385	1.394	C3–C2–C7	119.4	119.6
C2–C7	1.390	1.400	C2–C3–C4	118.6	118.7
C3–C4	1.381	1.390	C3–C4–C5	123.1	122.8
C4–C5	1.378	1.389	C3–C4–N8	118.2	118.2
C5–C6	1.385	1.392	C5–C4–N8	118.8	119.0
C6–C7	1.382	1.392	C4–C5–C6	117.5	117.7
N8–O9	1.187	1.225	C5–C6–C7	120.8	120.8
N8–O10	1.186	1.223	C2–C7–C6	120.6	120.3
N18–O19	1.167	1.199	C4–N8–O9	117.6	117.6
N18–O20	1.189	1.222	C4–N8–O10	117.5	117.6
N18–O21	1.321	1.382	O9–N8–O10	125.0	124.8
			O19–N18–O20	127.8	128.2
			O19–N18–O21	115.5	115.0
			O20–N18–O21	116.7	116.7

3.2 Mulliken charge analysis

The mulliken atomic charges of 3NAN given in Table 3 and the histogram is shown in Fig. 4. By quantum chemical methods, Mulliken atomic charge distribution was calculated, which has a vital role to the molecular system because atomic charges effect dipole moment, polarizability and electronic structure (Siva et al. 2017b). The hydrogen atom (H11) (0.497e in HF and 0.451e in B3LYP) in HNO_3 group of 3NAN was more electropositive, this hydrogen atom was attached with electronegative atoms (N18, O19, O20, O21). Also, nitrogen atom has more electro negativity (N1) (-0.535e in HF and -0.474e in B3LYP), this nitrogen atom enclosed by H12 and H13 (electropositive atom) and C2 (carbon atom).

3.3 Vibrational analysis

The 3NAN consists of 21 atoms, with 57 modes of vibrations. The comparison of experimental and computed IR and Raman spectra of 3NAN are given in Fig. 5 and frequency values are given in Table 4.

3.3.1 NH$_2$ vibrations

The NH$_2$ group vibrations are expressed as antisymmetric stretching, symmetric stretching, scissoring, wagging, rocking and twisting vibrations are spread over a region in the spectrum (Siva et al. 2017a). In theoretical spectrum the peak at 3826 cm^{-1} in HF and 3596 cm^{-1} in B3LYP method are assigned to NH$_2$ antisymmetric stretching.

Table 3 Computed atomic charges of 3NAN

Atoms connected	HF/6–311 + +G(d,p)	B3LYP/6–311 + +G(d,p)
N1	− 0.535	− 0.474
C2	0.027	− 0.007
C3	− 0.152	− 0.259
C4	0.036	− 0.224
C5	− 0.134	0.071
C6	− 0.119	− 0.222
C7	− 0.552	− 0.151
N8	− 0.120	− 0.185
O9	− 0.048	− 0.002
O10	− 0.056	− 0.005
H11	0.497	0.451
H12	0.317	0.282
H13	0.294	0.288
H14	0.274	0.229
H15	0.274	0.239
H16	0.241	0.201
H17	0.182	0.166
N18	− 0.141	− 0.330
O19	− 0.052	0.014
O20	− 0.125	− 0.035
O21	− 0.106	− 0.048
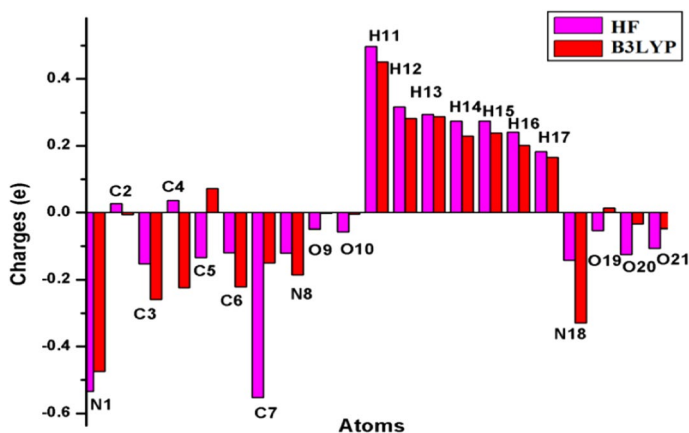
Fig. 4 Histogram of atomic charges on 3NAN by HF and B3LYP methods

NH_2 symmetric stretching wavenumbers are calculated at 3742 and 3510 cm^{-1} in HF and B3LYP respectively. NH_2 scissoring are calculated at 1808 and 1654 cm^{-1} in HF and B3LYP respectively. NH_2 twisting is calculated at 1628 and 1494 cm^{-1} in HF and B3LYP respectively. NH_2 wagging along with scissoring NO_2 vibrations are observed as weak peak at 1036 in Raman and theoretically scaled by HF and B3LYP at 1037 and
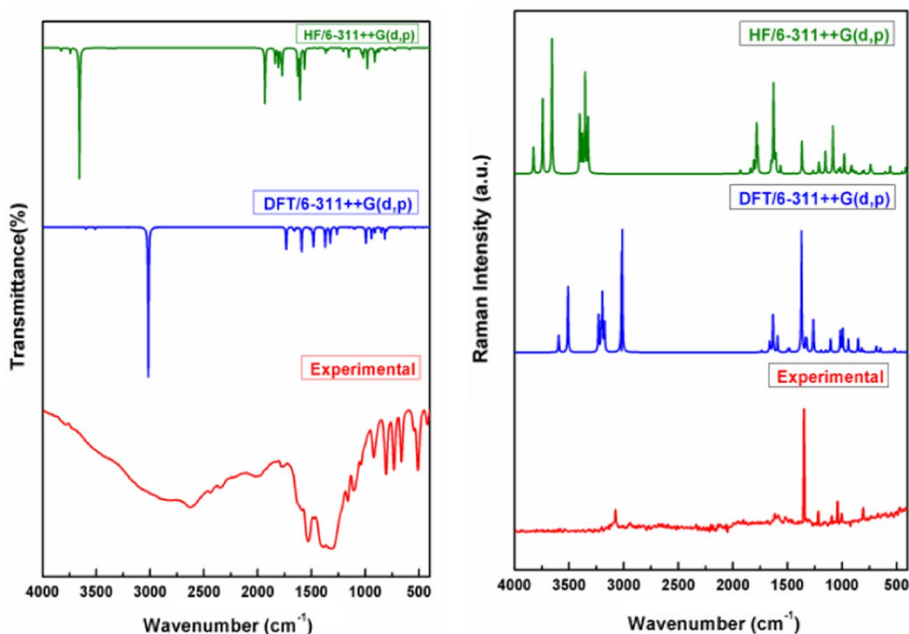
Fig. 5 Experimental and computed IR & Raman spectra of 3NAN

942 cm^{-1} respectively. The rocking NH$_2$ vibrations are calculated at mode 34 corresponding experimental spectrum identified as a weak peak in Raman at 1198 cm^{-1} and a medium peak at 1174 cm^{-1} in IR.

3.3.2 NO$_2$ vibrations

In nitrobenzene and substituted nitrobenzene, the band around 1500–1570 cm^{-1} and 1300–1370 cm^{-1} are represents the asymmetric and symmetric stretching vibrations of NO$_2$ group, respectively (Prabavathi et al. 2013). The NO$_2$ asymmetric stretching vibrations are theoretically computed by HF and B3LYP at 1772 and 1591 cm^{-1} respectively. The NO$_2$ symmetric stretching vibration theoretically scaled by HF and B3LYP method at 1367 and 1325 cm^{-1}, respectively. The scissoring NO$_2$ vibrations are observed as weak peak at 1036 cm^{-1} computed at mode 30 and mode 4 represents NO$_2$ twisting vibrations in theoretical calculation.

3.3.3 C–C and C–N vibrations

The title compounds have C–C and C–N stretching vibrations is usually occur in the region 1300–1600 cm^{-1}. In theoretical spectrum the peak at 1837 cm^{-1} by HF and

Table 4 The experimental (FT-IR, FT-Raman) and calculated frequencies of 3NAN with their vibrational assignments

Mode number	Experimental frequency (cm^{-1})		Calculated frequency (cm^{-1})						Vibrational assignments
			HF/6–311 + +G(d,p)			B3LYP/6–311 + +G(d,p)			
	FT-IR	Raman	ν_{cal}	$^a I^{IR}$	$^b I^{Raman}$	ν_{cal}	$^a I^{IR}$	$^b I^{Raman}$	
1			7	1.608	0.677	14	2.508	1.518	Lattice vibration
2			20	0.567	3.971	23	4.937	3.3284	Lattice vibration
3			31	0.519	4.935	38	0.016	5.444	t (NO_2)
4			41	0.185	0.204	46	0.067	0.4355	t (NO_2)
5			80	1.181	1.195	83	0.126	1.2479	t (NO_2 of HNO_3)
6			93	2.415	0.967	92	1.970	1.1478	ρ (NH_2)
7			153	11.937	1.431	153	10.453	1.4687	Ring vibration
8			190	5.666	2.227	181	17.463	2.9798	γ (C–H)
9			236	2.515	0.487	217	1.630	0.5016	ρ (NH_2)
10			279	2.402	0.203	266	12.601	0.1362	ω (NH_2)
11			383	10.033	0.472	363	4.609	3.1685	ρ (NH_2)
12			417	1.288	3.882	394	0.685	1.4698	ρ (NH_2) + ν (C–N)
13			451	1.584	1.411	431	1.455	0.1871	γ (C–H)
14			477	2.143	0.107	465	7.541	1.0761	t (NH_2)
15	518 m		558	0.207	4.909	518	1.328	4.4912	β (C–C)
16			587	19.027	0.288	537	16.845	0.4917	γ (C–C)
17			605	1.200	1.477	563	1.320	1.1435	β ((C–C) + NH_2)
18	668 m		724	27.030	1.363	648	5.888	5.2998	β (O–H)
19			730	8.647	1.558	673	27.446	0.2197	γ (C–H)
20	736 m		741	9.985	5.824	684	3.007	4.0857	δ (NO_2 of HNO_3) + ν (N–O of HNO_3)
21			798	16.302	2.257	688	2.584	4.3759	β (C–C)
22	829 m	806 w	814	18.377	1.613	727	10.487	1.0618	ω (NH_2) + γ (C–H + N–O)
23			871	39.206	1.663	784	10.796	0.4096	γ (N–O of HNO_3) + β (C–H)
24			894	46.143	2.167	800	48.280	1.5888	γ (C–H + O–H + N–H)

Table 4 (continued)

Mode number	Experimental frequency (cm^{-1})		Calculated frequency (cm^{-1})						Vibrational assignments
			HF/6–311++G(d,p)			B3LYP/6–311++G(d,p)			
	FT-IR	Raman	ν_{cal}	^{a}I IR	^{b}I Raman	ν_{cal}	^{a}I IR	^{b}I Raman	
25			911	150.048	4.778	818	165.006	5.4327	γ (C–H+O–H+N–H)
26	921 w		919	9.882	2.909	852	74.620	16.878	γ (C–H+O–H+N–H)
27			980	229.064	13.410	910	77.287	1.4858	γ (C–H)
28			1018	105.262	4.118	932	5.485	0.4155	γ (C–H)
29			1031	53.028	2.216	940	63.773	1.8888	ω (NH$_2$) + ν (C–N+N–O) + δ (NO$_2$)
30		1036 w	1037	26.058	1.744	942	110.273	15.1187	ω (NH$_2$) + δ (NO$_2$ + NO$_2$ of HNO$_3$) + ν (O–N)
31			1083	5.662	33.291	993	225.799	29.5752	γ (O–H)
32		1082$_w$	1110	0.430	0.129	998	1.405	0.5063	γ (C–H)
33	1105 m		1152	106.961	14.764	1016	7.718	27.1688	β (C–C) + δ (NH$_2$)
34		1198 w	1155	1.212	1.882	1094	16.099	0.3468	β (C–H) + ρ (NH$_2$)
35	1174 m		1204	38.954	1.737	1105	21.963	17.2829	β (C–H+C–C)
36			1211	5.906	7.893	1148	9.808	3.0772	ρ (NH$_2$) + β (C–H)
37			1265	2.534	2.355	1192	0.514	2.704	β (C–H)
38	1324 w	1359 s	1349	24.703	1.378	1263	102.150	43.7652	ν (C–N) + β (C–C)
39			1367	57.057	23.989	1325	214.008	14.5075	ν (C–N) + ν_s (NO$_2$)
40			1444	6.034	0.707	1333	47.100	16.056	ν (C–N) + ν_s (NO$_2$ HNO$_3$) + β (C–H)
41	1531 s		1563	230.085	6.124	1366	43.761	8.9454	ν (C–C+C–N) + ρ (NH$_2$)
42			1607	513.942	10.079	1372	268.421	165.089	ν (C–N) + ν_s HNO$_3$
43			1611	98.852	7.524	1482	275.940	5.4486	β (O–H of HNO$_3$)
44			1628	284.981	69.752	1494	60.513	5.1155	ν (C–C) + t (NH$_2$)
45			1647	2.153	7.674	1516	23.302	0.3785	ν (C–C) + β (C–H)
46			1772	285.838	17.106	1591	350.399	24.3597	ν_{as} NO$_2$ + ν (C–C+C–N) + β (C–H)

Table 4 (continued)

Mode number	Experimental frequency (cm⁻¹)		Calculated frequency (cm⁻¹)						Vibrational assignments
	FT-IR	Raman	HF/6–311++G(d,p)			B3LYP/6–311++G(d,p)			
			ν_{cal}	a I IR	b I Raman	ν_{cal}	a I IR	b I Raman	
47			1782	125.991	38.190	1632	13.773	55.4454	ν (C–C) + β (C–H + N–H)
48			1808	206.041	10.298	1654	46.729	3.0565	δ (NH$_2$)
49			1837	168.388	4.332	1665	40.797	15.5683	δ (NH$_2$) + ν (C–C + C–N + N–O)
50	2003 w		1932	618.427	3.249	1735	314.009	3.0517	ν_{as} HNO$_3$
51		3073 w	3326	7.812	65.555	3016	2106.123	315.5617	ν (O–H of HNO$_3$)
52			3353	7.523	118.434	3176	2.519	60.9266	ν (C–H)
53			3380	5.044	43.703	3194	3.565	123.6094	ν (C–H)
54			3402	4.013	69.781	3207	4.951	53.6183	ν (C–H)
55			3657	1428.708	173.243	3230	4.025	80.2772	ν (C–H)
56			3742	60.245	98.258	3510	29.025	153.0756	ν_s (NH$_2$)
57			3826	31.359	36.003	3596	27.115	40.4919	ν_{as} (NH$_2$)

w-weak; m- medium; vs—very strong; ν-stretching;

β- in plane bending; γ- out -of- plane bending; ν_s sym.stretching; ν_{as} asym.stretching; ρ -rocking; δ—scissoring; t- twisting; ω-wagging;

1665 cm^{-1} in B3LYP method are assigned to C–C stretching vibrations. Similarly, C–N stretching vibrations are assigned to 1444 cm^{-1} in HF and 1333 cm^{-1} in B3LYP.

3.3.4 C-H vibrations

In 3NAN, the C–H stretching vibrations confirm aromatic structure. These stretching vibrations are occurs in the characteristic region around 3100 cm^{-1}B (Bhuvaneswari et al. 2018; Thangarasu et al. 2018). The C–H stretching vibrations peaks are assigned in the theoretical spectrum in the region 3657–3176 cm^{-1}. The in-plane bending vibrations are observed with O–H stretching in theoretical spectrum at 1782 cm^{-1} in HF and 1632 cm^{-1} in B3LYP.

3.3.5 Vibrations of nitrate anion

The title compound, NO_3^- asymmetric stretching vibrations are observed as a weak peak at 2003 cm^{-1} in IR and in theoretical spectrum at 1932 and 1735 cm^{-1} in the HF and B3LYP respectively. NO_3^- symmetric stretching vibrations are observed at 1607 and 1372 cm^{-1} in the HF and B3LYP respectively. The O–H stretching is observed as a weak peak in IR at 3073 cm^{-1}, it is scaled at 3326 cm^{-1} in HF and 3016 cm^{-1} in B3LYP. The O–H in-plane banding vibrations are calculated 1611 and 1482 cm^{-1} in the HF and B3LYP respectively. The O–H out-plane banding vibrations observed as a weak peak at 1082 cm^{-1} in IR and it is well matches with experimental spectra.

3.4 Frontier moleculer orbital analysis

In the organic molecules, optical and electric properties are proposed by using frontier molecular orbital analysis (Jean and Volatron et al. 2005; Drozd and Dudzic et al. 2013; Mary Novena et al. 2017). The molecular orbital have two important interactions; such as HOMO means the ability to donate an electron and LUMO represents accept an electron. Also, these orbitals are named as frontier orbitals. Frontier electron density (Palafox et al. 2000) is used to explain the several types of reaction in conjugated system and most reactive position in π-electron systems. Also, FMO plays an essential part in abiding chemical stability of the compound (Fleming et al. 1976). The calculated HOMO and LUMO energies and some important parameters of the 3NAN were calculated by HF and DFT/B3LYP method as shown in Table 5. The stimulated energy level diagrams of 3NAN molecule was

Table 5 Calculated energy values of 3NAN

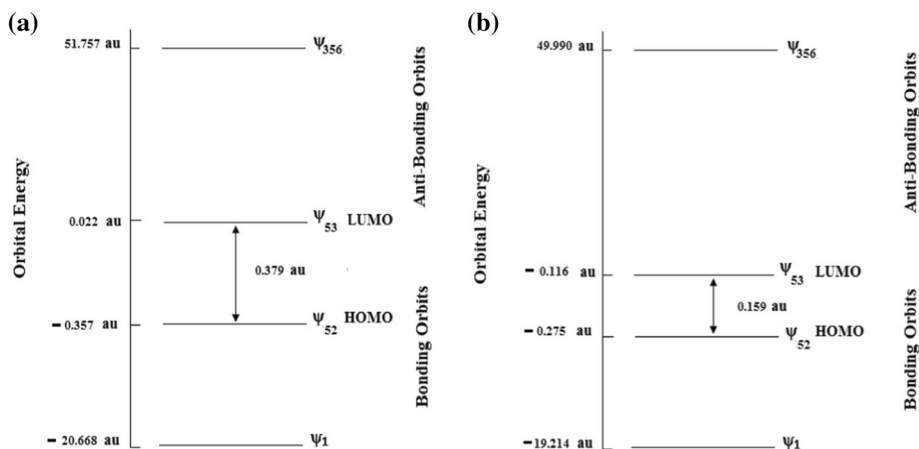| Parameters (a.u.)	HF 6–311 + + G(d,p)	B3LYP
HOMO	0.022	− 0.116
LUMO	− 0.357	− 0.275
$\Delta(E_{LUMO}–E_{HOMO})$	0.379	0.159
Electron affinity (A)	− 0.022	0.116
Ionization potential (I)	0.357	0.275
Chemical hardness (η)	0.190	0.080
Chemical potential (μ)	− 0.168	− 0.196
Electronegativity (χ)	0.168	0.196
Electrophilicity Index	0.074	0.240

(a)

(b)

Fig. 6 Molecular orbital energy level diagram of 3NAN by **a** HF and **b** B3LYP levels

shown in Fig. 6. A huge amount of charge transfer occurred in 3NAN is indicated by small energy gap, which is connected with a high chemical reactivity. The small value of energy gap and high value of charge transfer leads the molecules to biologically active.

For 3NAN, 356 energy levels are observed in the energy range −20.668 au to 51.757 au and −19.214 au to 49.990 au in HF and B3LYP method respectively. The calculated HOMO and LUMO energy values of 3NAN molecule in HF and B3LYP are −0.357/0.022 au and −0.275/−0.116 au repectively. The energy gap value between the frontier orbital was 0.379 a.u in HF and 0.159 a.u in B3LYP.

3.5 Thermal analysis

Thermal behaviour was analyzed by using simultaneous DTA/TGA analysis in the temperature range 30–650 °C in air atmosphere. The TGA/DTA curves of 3NAN are given in the Fig. 7. The TGA/DTA curve represent that the decomposition in the range of 190–650 °C. The three main stages of decomposition in 3NAN occurred within this temperature range as given Fig. 8. In TGA/DTA curve, weight loss 11% noted in temperature range 150–190 °C due to the elimination of water group from 3NAN, it indicates first stage of decomposition. The second stage of major weight loss 41% occurs at 190–220 °C temperature range, which is due to the liberation of NO and CO from the earlier intermediate compound. The next decomposition stage is owing to the removal of NO and C_2H_4 in the temperature range 220–420 °C with weight loss of 29%. An endothermic peak observed at 209 °C is may be the melting point of the compound. The soft exothermic peaks at 485 °C are due to the decomposition of the organic compound.

3.6 Antimicrobial activity analysis

To analyze the antimicrobial activity of 3NAN, the crystal was tested against Staphylococcus Aureus (G^{+ve}) and Klebsiella Pneumoniae (G^{-ve}) by disc diffusion method with 50 and 100 mg mL^{-1} concentrations. Similarly, the title compound antifungal activity was tested against Candida Albicans (C. albicans). The zone of inhibition were measured in diameter
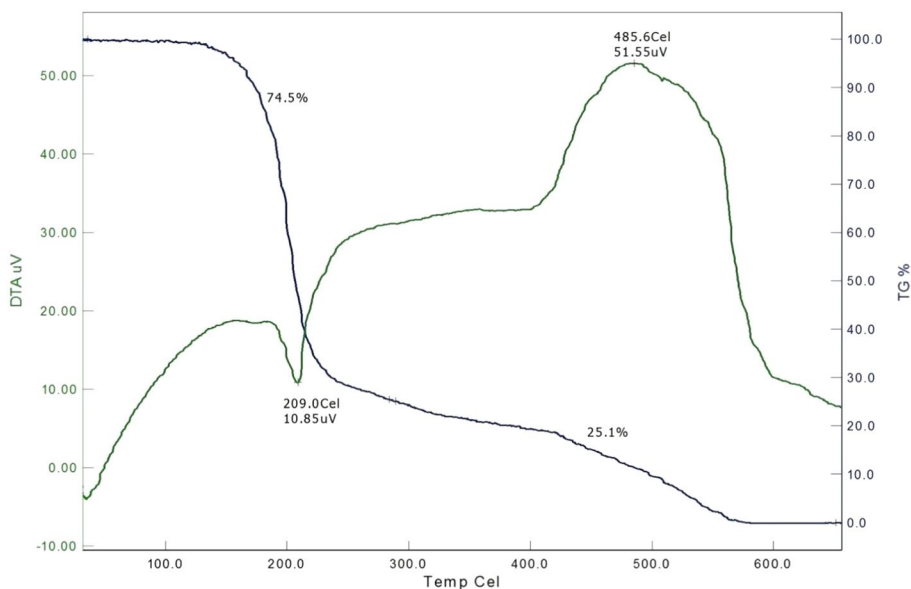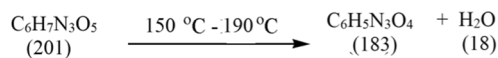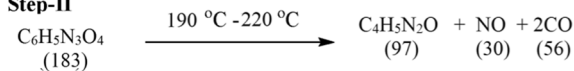
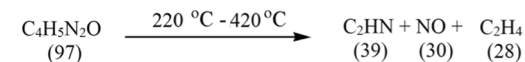**Fig. 7** DTA/TGA curve of 3NAN

Fig. 8 Decomposition steps of 3NAN

Step-I

$C_6H_7N_3O_5$ $\xrightarrow{\text{150 °C - 190 °C}}$ $C_6H_5N_3O_4$ + H_2O
(201)   (183)   (18)

Step-II

$C_6H_5N_3O_4$ $\xrightarrow{\text{190 °C -220 °C}}$ $C_4H_5N_2O$ + NO + 2CO
(183)   (97)   (30)   (56)

Step-III

$C_4H_5N_2O$ $\xrightarrow{\text{220 °C - 420 °C}}$ C_2HN + NO + C_2H_4
(97)   (39)   (30)   (28)

Note: The values given in parenthesis stand for the molecular weights of the respective species.

are shown in Table 6. The biological activity of 3-nitroanilinium nitrate complex results indicate, it is a moderately active material against all the organisms (Karthiga Devi et al. 2017; Chitradevi et al. 2015) (Figs. 9, 10, 11).

Fig. 9 The antibacterial activity
of 3NAN against Staphylococcus
Aureus

Fig. 10 The antibacterial activity
of 3NAN against Klebsiella
Pneumoniae

Fig. 11 The antifungal activity of
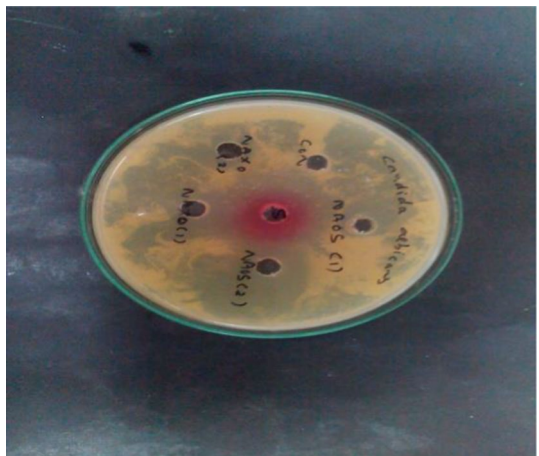3NAN against Candida Albicans

Table 6 Antibacterial and Antifungal activity of 3NAN compound against some human pathogens

Sample	Concentration (mg/ml)	Zone Of Inhibition In diameter (mm)		
		Micro organisms used		
		K. Neumoniae (G^{+ve})	S. Aureus (G^{-ve})	C. Albicans
3NAN	50	12	R	13
	100	12	R	13
SD	50/100	16	18	16

R, Resistant; SD-Standard drug (Antibacterial activity)–Amikacin; SD-Standard drug (Antifungal activity)–Ketokonazole

4 Conclusions

3-nitroanilinium nitrate was synthesized and characterized by various characterization techniques. The detailed interpretation of the vibrational spectra between calculated (IR, Raman) and computed spectra, experimental results of 3NAN molecule show the good reliability with computed results. The higher stability of the title molecule is confirmed from the computed HOMO–LUMO energy gap. TGA and DTA exposed about the material, thermal analysis confirmed the absence of phase transition before the material reach the melting point. Antimicrobial activity of the title compound was investigated.

Declarations

Conflict of interest The authors declared that they have no conflict of interest.

References

Becke, A.D.: Density-functional thermochemistry. III. The role of exact exchange. J. Chem. Phys. **98**, 5648–5653 (1993)

Bhuvaneswari, N., Priyadharsini, N., Sivakumar, S., Venkatachalam, K., Siva, V.: Growth, vibrational, optical, thermal, magnetic and dielectric behavior of organo-metallic tetramethyl ammonium cadmium chloride crystal. J. Therm. Anal. Calorim. **136**, 411–417 (2018)

Bishop, D.M., Champagne, B., Kirtman, B.: Molecular vibration and nonlinear optics. J. Chem. Phys. **109**, 9987–9994 (1998)

Chitradevi, A., Suresh Kumar, S., Athimoolam, S., Asath Bahadur, S., Sridhar, B.: Single crystal XRD, vibrational spectra, quantum chemical and thermal studies on a new semi-organic crystal: 4-Aminium antipyrine chloride. J. Mol. Struct. **1099**, 58–67 (2015). https://doi.org/10.1016/j.molstruc.2015.06.022

David, W.I.F., Shankland, K., Vandestreek, J., Pidcock, E., Motherwell, W.D.S., Cole, J.C.: DASH: a program for crystal structure determination from powder diffraction data. J. Appl. Cryst. **39**, 910–915 (2006)

Dennington, R., Keith, T., Millam, J., Gauss View Version 5.0.8 Semichem Inc., Shawnee Mission KS, (2013)

Drozd, M., Dudzic, D.: Guanidinium perchlorate ferroelectric crystal. Study of vibrational properties based on experimental measurements and theoretical calculations. Spectrochim. Acta Part A **115**, 345–356 (2013). https://doi.org/10.1016/j.saa.2013.06.023

Fleming, I.: Frontier Orbitals and Organic Chemical Reactions. John Wiley & Sons, New York (1976)

Frisch, M.J., Trucks, G.W., Schlegel, H.B., Scuseria, G.E., Robb, M.A., Cheeseman, J.R., Scalmani, G., Barone, V., Mennucci, B., Petersson, G.A., Nakatsuji, H., Caricato, M., Li, X., Hratchian, H.P., Izmaylov, A.F., Bloino, J., Zheng, G., Sonnenberg, J.L., Hada, M., Ehara, M., Toyota, K., Fukuda, R., Hasegawa, J., Ishida, M., Nakajima, T., Honda, Y., Kitao, O., Nakai, H., Vreven, T., Montgomery, J.A., Jr., Peralta, J.E., Ogliaro, F., Bearpark, M., Heyd, J.J., Brothers, E., Kudin, K.N., Staroverov, V.N., Kobayashi, R., Normand, J., Raghavachari, K., Rendell, A., Burant, J.C., Iyengar, S.S., Tomasi, J., Cossi, M., Rega, N., Millam, J.M., Klene, M., Knox, J.E., Cross, J.B., Bakken, V., Adamo, C., Jaramillo, J., Gomperts, R., Stratmann, R.E., Yazyev, O., Austin, A.J., Cammi, R., Pomelli, C., Ochterski, J.W., Martin, R.L., Morokuma, K., Zakrzewski, V.G., Voth, G.A., Salvador, P., Dannenberg, J.J., Dapprich, S., Daniels, A.D., Farkas, O., Foresman, J.B., Ortiz, J.V., Cioslowski, J., Fox, D.J.: Gaussian 09, Revision B.01. Gaussian Inc., Wallingford (2010)

Hohenberg, P., Kohn, W.: Inhomogeneous electron gas. Phys. Rev. B **136**, 864–871 (1964)

Jain, A.K., Mehta, S.C., Shrivastava, N.M.: Hypoglycemic and antihyperglycemic effects of newly synthesized sulfonyloxy derivatives of azalactone in normal and alloxan diabetic rabbits. Indi. J. Pharmaco. **37**, 395–396 (2005)

Jean, Y., Volatron, F.: An Introduction to Molecular Orbitals. Oxford University Press, Oxford (2005)

Karthiga Devi, P., Venkatachalam, K.: Growth, spectroscopic, mechanical, thermal, antimicrobial and DFT studies of piperidinium hydrogen oxalate. J. Mater Sci: Mater Electron. **28**, 8061–8073 (2017). https://doi.org/10.1007/s10854-017-6512-7

Krishnakumar, V., Nagalakshmi, R.: Terahertz generation in 3-Nitroaniline single crystals. Cryst. Growth Des. **8**, 3882–3884 (2008)

Lee, C., Yang, W., Parr, R.G.: Development of the Colle-Salvetti correlation-energy formula into a functional of the electron density. Phys. Rev. **37**, 785–789 (1988)

Mary Novena, L., Suresh Kumar, S., Athimoolam, S., Saminathan, K., Sridhar, B.: Single crystal, vibrational and computational studies of Theophylline (a bronchodilator drug) and its chloride salt. J. Mol. Struct. **1133**, 294–306 (2017). https://doi.org/10.1016/j.molstruc.2016.11.087

Palafox, M.A.: Scaling factors for the prediction of vibrational spectra. I. Benzene molecule. Int. J. Quant. Chem. **77**, 661–684 (2000)

Prabavathi, N., Nilufer, A., Krishnakumar, V.: Spectroscopic (FT-IR, FT-Raman, UV and NMR) investigation, conformational stability, NLO Properties, HOMO-LUMO and NBO Analysis of Hydroxyquinoline Derivatives by Density Functional Theory Calculations. Spectrochim. Acta A **114**, 449–474 (2013). https://doi.org/10.1016/j.saa.2013.05.011

Reis, H., Papadopoulos, M.G., Calaminici, P., Jug, K., Köster, A.M.: Calculation of macroscopic linear and nonlinear optical susceptibilities for the naphthalene, anthracene and meta-nitroaniline crystals. Chem. Phys. **261**, 359 (2000)

Schlegel, H.B.: Optimization of equilibrium geometries and transition structures. J. Comput. Chem. **3**(2), 214–218 (1982)

Siva, V., Shameem, S., Suresh Kumar, S., Raja, M., Athimoolam, S., Asath Bahadur, S.: Structural, spectral, Quantum chemical and thermal studies on a new NLO crystal: Guanidinium Cinnamate. J. Mat. Sci: Mat. Electr. **28**, 12484–12496 (2017a). https://doi.org/10.1007/s10854-017-7070-8

Siva, V., Suresh Kumar, S., Suresh, M., Raja, M., Athimoolam, S., Asath Bahadur, S.: N-H•••O hydrogen bonded novel nonlinear optical semiorganic crystal (4-methoxyanilinium trifluoroacetate) studied through theoretical and experimental methods. J. Mol. Struct. **1133**, 163–171 (2017b). https://doi.org/10.1016/j.molstruc.2016.11.088

Siva, V., Asath Bahadur, S., Shameem, A., Murugan, A., Athimoolam, S., Suresh, M.: Supramolecular architecture, hydrogen bonding assembly and Hirshfeld surface analysis of charge transfer adipate salt of 4-methoxyaniline. Chem. Data Collect. **24**, 100281 (2019)

Thangarasu, S., Siva, V., Athimoolam, S., Asath Bahadur, S.: Molecular structure, spectroscopic and quantum chemical studies on benzoic acid and succinic acid co-crystals of 2-Aminopyrimidine. J. Theor. Comput. Chem. **17**(4), 1850021 (2018)